PIV with volume lighting in a narrow cell: An efficient method to measure large velocity fields of rapidly varying flows

Matthieu Roudet [a], Anne-Marie Billet [a], Frédéric Risso [b], Véronique Roig [b,*]

[a] LGC, Université de Toulouse (INPT, UPS) and CNRS. 4 Allée Emile Monso, BP74233, Toulouse Cedex 4, 31432, France
[b] IMFT, Université de Toulouse (INPT, UPS) and CNRS. Allée Camille Soula, Toulouse 31400, France

A B S T R A C T

In this work we test a methodology for PIV measurements when a large field of view is required in planar confined geometries. Using a depth of field larger than the channel width, we intend to measure the in-plane variations of the velocity of the fluid averaged through the width of the channel, and we examine in which operating conditions this becomes possible. Measurements of the flow through a narrow channel by PIV are challenging because of the strong velocity gradients that develop between the walls. In particular, all techniques that use small particles as tracers have to deal with the possible migration of the tracers in the direction perpendicular to the walls. Among the complex mechanisms for migration, we focus on the so called Segré–Silberberg effect which can lead to transverse migration of neutrally buoyant tracers of finite size. We report experimental PIV measurements in a Hele-Shaw cell of 1 mm gap, which have been carried out by using neutrally buoyant tracers of size around 10 μm. By considering steady flows, we have observed, in particular flow regimes, the effect of an accumulation of the tracers at a certain distance to the wall due to the so called Segré–Silberberg effect. The particle migration is expected to occur at any Reynolds numbers but the migration velocity depends on the Reynolds number. A significant migration therefore takes place each time the observation duration is large enough compared to the migration time. For a given observation duration, the tracers remain uniformly distributed at low Reynolds numbers whereas they all accumulate at the equilibrium position at large ones. When using volume lighting, the PIV algorithm provides the average velocity of the flow through the gap at low Reynolds number, while it leads to the velocity of the flow at the equilibrium position of the tracers at large Reynolds numbers. By considering unsteady flows, we have observed that the migration does not occur if the timescale of flow variation is short compared to the time required for the parabolic flow to develop across the gap. In this case, there is no transverse velocity gradient and the PIV algorithm provides the fluid velocity. Altogether, these results allow us to propose guidelines for the interpretation of PIV measurements in confined flow, which are based on the theoretical predictions of the tracer migration derived by Asmolov [1].

1. Introduction

With the recent development of micro-reactor engineering, the experimental study of transport and mixing phenomena in narrow channels is a new technical challenge [2,3]. Conventional PIV investigations use light sheet illumination ([4–6] in microchannel). For narrow channels however, the lack of optical access leads to front illumination (or volume illumination) of the flow [7,8]. Using this technique, all tracers distributed over the channel width are lighted. There are two ways of filming these seeding particles with the aim of performing PIV measurements. One consists in using camera optics with a depth of field that is small compared to the channel thickness; in that way the optical acquisition system must be adjusted to detect only the tracers located at a given distance from the walls [7,9]. The drawbacks of this method are its limitation to small measurement windows and a possible lack of tracers in the measuring plane. A more convenient solution is to use camera optics with a depth of field larger than the channel width. In this case, all the tracers laying in the field of view of the camera are well-focused and contribute to the velocity measurement [8]. Two other difficulties however arise, which have to be considered to make sure that the PIV measurements are relevant. The first concerns the PIV algorithm: while the fluid velocity ranges from zero at the wall to the maximum velocity at the middle of the channel width, velocity gradients at the scale of the PIV interrogation domain may decrease the amplitude of the displacement correlation peak and enlarge its width, reducing its detectability and

* Corresponding author. Tel.: +33 (0)5 34 32 28 20; fax: +33 (0)5 34 32 29 91.
E-mail address: roig@imft.fr (V. Roig).

generating random errors on its localisation [10]. The second and major difficulty comes from a possible migration of the tracers in the direction perpendicular to the walls, which has been observed even for neutrally-buoyant particles because of the non-uniformity of the velocity [11].

Experimental tests are therefore required to assess the use of a PIV technique when volume lighting is used together with a large optical depth of field. In this article, we investigate the liquid flow within a Hele-Shaw cell by using a frontal lighting and an optical depth of the camera larger than the cell gap. Contrasted configurations are investigated by varying the Reynolds number of the channel and the timescale of flow variations. The article is organized as follows. The experimental set-up and the PIV system are described in the next section. Results concerning the case of a steady flow are first presented. Then, the response of the PIV system to time-varying flow is investigated. Finally, the results obtained about the influence of velocity gradients and tracer migrations will allow us to draw guidelines for the use of the PIV technique is such configurations.

2. Experimental facility and instrumentation

The cell consists of two vertical glass plates of 400 mm width, 800 mm height and 8 mm thick, which are separated by a thin gap δ = 1 mm (Fig. 1). It is filled with distilled water and open to atmosphere at the top. At the bottom, evacuation valves have been regularly distributed all along the cell. The valves are used to empty the cell at various rates with the aim of generating a uniform flow in the central part of the channel. Capillary tubes of different diameters can also be inserted at the bottom in order to inject bubbles of various diameters. In this article, both the uniform flow and that induced by a single rising bubble will be used as reference configurations to investigate the role of tracer migration on PIV measurements.

The present PIV method uses front lighting of the measurement window (Fig. 2). A Quantel multipulse Nd:YAG laser of 2 $\times$ 200 mJ generates a light beam that is made divergent by means of a spherical lens. The laser axis makes an angle of about 30° relative to the perpendicular direction of the cell in order to avoid direct reflexion of the light back to the laser cavity and direct light on the camera. The whole liquid vein corresponding to the intersection of the cone

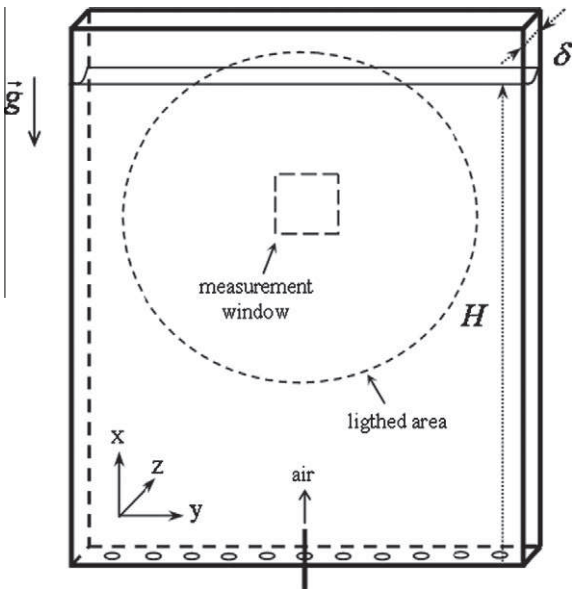

Fig. 1. Schematic of the Hele-Shaw cell.

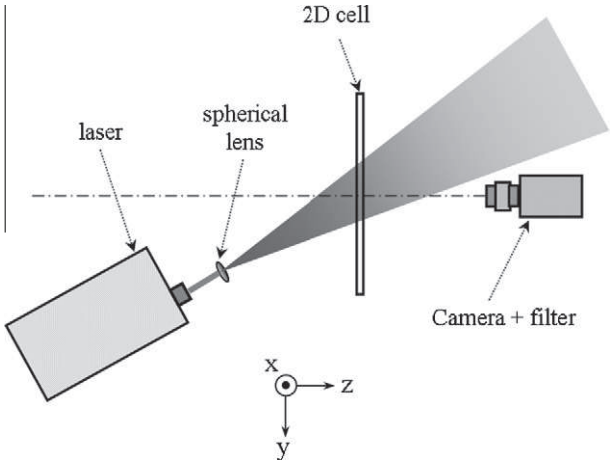

Fig. 2. Top view of the PIV set-up.

of light with the cell is illuminated. The lighted region is a disk of 400 mm diameter, much larger than the PIV measurement window, which is 59 mm width and 74 mm height. This ensures an appropriate uniformity of the light intensity within the measurement window, with variations smaller than 5%. The tracers are fluorescent particles made of B-Rhodamine encapsulated in a PMMA membrane. Fig. 3 shows their distribution of size measured by means of a Malvern Mastersizer granulometer: the diameters $2a$ range from 3 to 25 μm with a median value of 10 μm. The tracers are therefore much smaller than the cell gap ($2a/\delta < 0.01$). They are added to the water before the filling of the cell. Their sedimentation velocity, which has been measured inside the cell in the absence of any flow, is 3×10^{-2} mm s^{-1}. It is much smaller than the characteristic flow velocities under consideration in this work, which range between 1 and 200 mm s^{-1}. When excited by the laser light at 532 nm, the tracers fluoresce at a wavelength centered around 570 nm. The tracer emission is recorded by means of a PCO 12-bits CCD camera (1280 $\times$ 1024 pixel) that faces the cell. The camera is equipped with a 580-nm high-pass filter in order to reduce the noise generated by reflections of the incident light, and with optics giving a depth of field larger than the cell gap. All tracers belonging to the measurement window hence contribute to the light intensity of recorded images, whatever their location within the gap. In other words, no distinction is made between slow tracers that are close to the cell walls and rapid

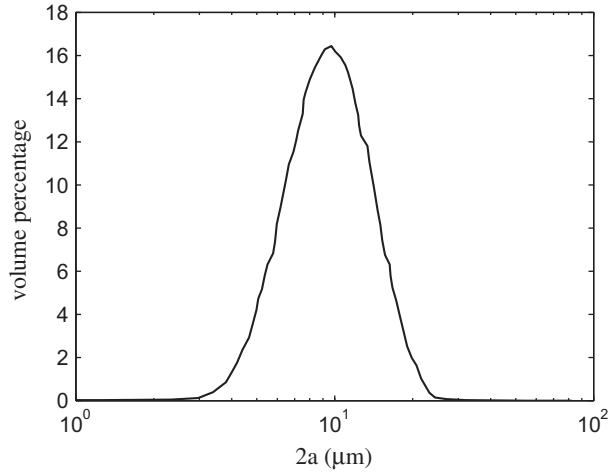

Fig. 3. Distribution of the diameter $2a$ of the tracer particles.

tracers that are in the middle of the gap. The frequency of PIV measurements was typically 5–10 Hz. The double-pulse laser system was synchronized with the camera. The delay between the two laser pulses was chosen for each measurement to satisfy accurate displacement measurement. The laser shot duration (about 5–7 ns) fixed the light acquisition. Indeed, the first image was obtained with the camera open for a delay of 11 μs containing the first laser-shot, and the second image, delayed of 1 μs from the first one, was obtained with the camera open for the rest of time between two PIV measurements containing the second laser shot. A raw image of the field of tracers seen by the camera is plotted in Fig. 4. Individual tracers cannot be detected, because their size is lower than a pixel, but the contrast and texture of this image is satisfactory for PIV measurements.

A two-dimensional velocity field $U_{PIV}(x,y,t)$ is computed from the recorded pairs of images by means of the software *PIVIS* developped at IMFT, which is based on an iterative multi-pass PIV algorithm [12,13], the precision of which has been checked to be better than 0.1 pixel. The computation involves two steps. First, the intercorrelation of the two raw images of each pair is calculated using interrogation cells of 64×64 pixels. Second, an iterative subpixel interpolation is performed and the final intercorrelation is computed using interrogation cells of 32×32 pixels with an overlapping of 50%. The measurement parameters have been adjusted to optimize the accuracy of the PIV algorithm. The concentration of tracers has been chosen in order to obtain about 15 tracers in each final interrogation cell. Due to the PIV algorithm and the mean size of the images of the tracers (around 3 pixels) we observed no peak locking. The time interval between the two images has been adjusted to lead to displacements ranging between 1/20 and 1/8 of the interrogation cell. We checked for all measurements that the displacement correlation peak clearly emerged from the secondary peaks and was sharp enough to allow unambiguous localisation of the maximum. In an instantaneous PIV field, only displacement vectors corresponding to a main correlation peak at least twice higher than secondary ones have been validated, the few others being removed and replaced by linear interpolations of validated ones. For investigation of the flow around a bubble, measurements obtained at less than 2 mm from a gas–liquid interface have been discarded because of the noise induced by reflexion. The accuracy of PIV measurement was estimated from r.m.s values during uniform flow generated by emptying. It is around ±3%.

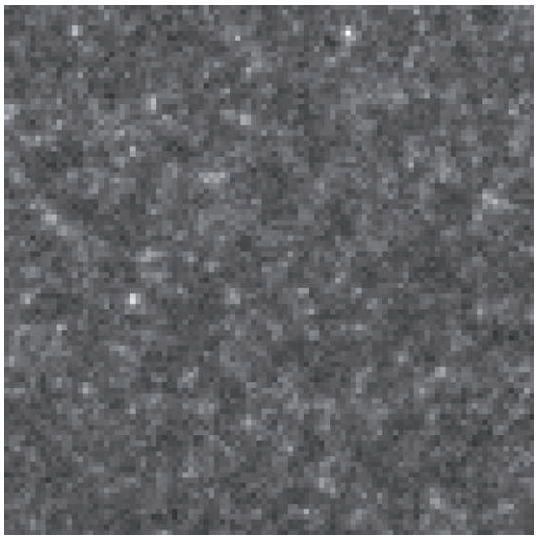

Fig. 4. Image of the field of tracers to be processed by PIV algorithm (100×100 pixels, 60 grey levels).

3. PIV measurements in a uniform steady flow

3.1. Experimental procedure and results

Since the velocity of a tracer depends on its location z within the gap, we do not a priori know how to interpret the velocity $U_{PIV}(x,y,t)$ provided by the present PIV method. Our objective is to calibrate $U_{PIV}(x,y,t)$ in a situation where the true velocity field $U(x,y,z,t)$ is known. This reference flow is obtained by emptying the cell via the discharging valves located at the bottom. The instant the valves are open is hereafter considered as the origin of time. The opening of the valve, operated manually, was rapid enough to be considered as instantaneous for the present purpose. The camera and the laser were started before we opened the valve in order to detect the instant when the fluid is set in motion taken as the origin of time. In the measurement window located in the middle of the cell in the horizontal y direction and 560 mm above the bottom, the liquid velocity U is uniform over the measurement plane (x,y). Its value $\langle U(t)\rangle$ averaged over the z direction is equal to the vertical velocity V of the free surface. The location of the gas–liquid interface is detected by digital image processing of the same images that are used for PIV; the velocity V is then obtained by time derivation with an accuracy of ±2%. In the z direction, a Poiseuille flow develops since we are considering laminar flows with channel Reynolds numbers, $Re_c = \langle U\rangle\delta/\nu$, less than 200. This flow takes a time $T_p = (\delta/2)^2/\nu \approx 0.25$ s to be developed. The circles in Fig. 5 show the time evolutions of interface velocity V for two runs at $Re_c = 28$ and 148. Note that V is only known from the instant T when free surface reaches the measurement window: $T = 1.6$ s for the largest discharging rate and is larger for slower discharges. Due to the decrease of the liquid height H above the discharging valve, the emptying velocity slightly decreases. However, the timescale of this velocity variation, $T_{var} = U(dU/dt)^{-1}$, is at least of 8 s. Finally, since $T/T_p \geqslant 8$ we can conclude that a Poiseuille flow exists at T when PIV and interface velocity are simultaneously measured, and as $T_{var}/T_p \geqslant 32$, this Poiseuille flow is quasi-steady. The calibration of the PIV technique is therefore done in a case where $U(z,t)$ adopts a parabolic profile with an average velocity, $\langle U\rangle = V$, that slightly decreases with time.

This configuration is thus particularly suitable to investigate the results provided by the PIV method in a steady flow. Fig. 5 also displays the value $U_{PIV}(t)$ obtained by averaging $U_{PIV}(x,y,t)$ over the measurement window. The PIV velocity is in good agreement with the reference velocity V for $Re_c = 28$ (Fig. 5a) whereas it is much smaller for $Re_c = 148$ (Fig. 5b). Fig. 6 presents the evolution of the ratio U_{PIV}/V for all investigated values of Re_c. The results show that the PIV velocity is equal to the liquid velocity averaged over the gap for $Re_c < 80$ while it is much smaller for $Re_c \geqslant 150$. This under-estimation of the averaged velocity by the PIV method at large Reynolds numbers may depend on the spatial distribution of tracers within the gap. We discuss this point in the following part.

3.2. Interpretation

Even if the tracer concentration is uniform at initial time, there is no guarantee that it will remain uniform all along an experiment. It is well-known that a buoyant particle in a vertical channel experiences a lift force, which results of the combined effects of the particle slip velocity and of the shear stress [14]. However, even a neutrally buoyant particle migrates laterally in a Poiseuille flow under the action of inertial forces, as it was observed first by Segré and Silberberg [11]. This effect depends on the channel Reynolds number Re_c and on the ratio a/δ of the particle size over the channel thickness (or tube diameter). It was described theoretically by Schonberg and Hinch [15] and then Asmolov [1], and investigated experimentally in a pipe flow by Matas et al. [16] for

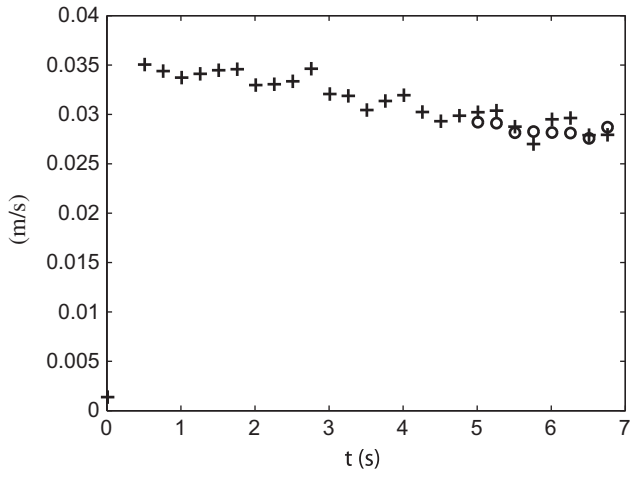

(a) $Re_c = 28$.

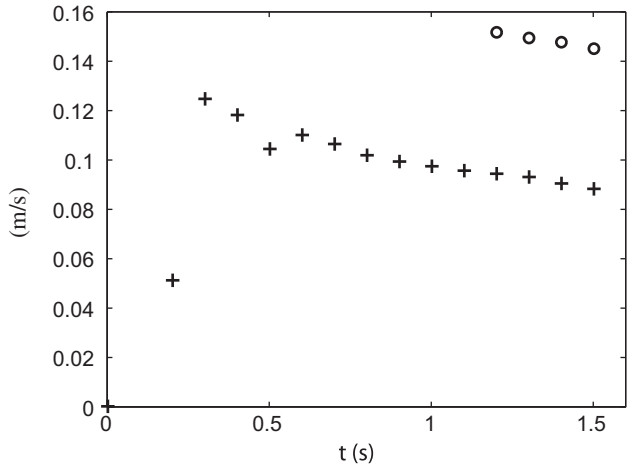

(b) $Re_c = 148$.

Fig. 5. Time evolution of the liquid velocity in the cell during emptying experiments for two different Reynolds numbers: + PIV measurements U_{PIV}, ∘ reference velocity V.

$67 \leqslant Re_c \leqslant 1700$. For a review of the literature in microchannels, the reader is referred to Kim and Yoo [17].

We will use the predictions provided by Asmolov [1] to interpret the present results. Asmolov used asymptotic expansions by assuming that the Reynolds number based on the tracer size and the strain rate, $Re_p = Re_c(a/\delta)^2$, is small while the channel Reynolds number Re_c remains finite. Two contributions to the lift force are identified. First the disturbance generated by the particle breaks the symmetry of flow on both sides of the particle, which generates a lift force that pushes the particle towards the walls. Note that this first lift force requires that the curvature of the velocity profile is non-zero. The second contribution to the lift force is due to the presence of the wall. In the layer between the wall and the particle, wall-induced inertia becomes significant and pushes the particle towards the middle of the channel. The first contribution is predominant in the middle of the channel while the second one is predominant close to the wall. Whatever its initial position, a particle migrates towards an equilibrium location z_{eq} where the two opposite lift forces are balanced. It is interesting to notice that the location where the particles accumulated in the experiment of Matas et al. [16] are in good agreement with the theory for $a/\delta = 1/42$ while it is moved towards the pipe axis for $a/\delta \geqslant 1/17$. In the present work, considering that the median value of the size distribution is $a/\delta = 1/200$, we may expect that the particles are small enough for the theory to be valid. Fig. 7 shows the Asmolov prediction of z_{eq} for the present range of Reynolds number (our origin of z_{eq} corresponds here to the middle of the channel). We observe that z_{eq}/δ monotonically depends on the Reynolds number and that it increases (i.e. equilibrium position moves towards the wall) from 0.32 to 0.40 as Re_c increases from 13 to 200.

To compare this prediction with the PIV measurements, we need to compute the tracer velocity, V_{tr}. Assuming that all tracers have accumulated at the equilibrium position and that the liquid flow is parabolic yields

$$\frac{V_{tr}}{\langle U \rangle} = \frac{3}{2}\left(1 - 4\left(\frac{z_{eq}}{\delta}\right)^2\right). \tag{1}$$

The theoretical result (1) is represented by the curve added on Fig. 6. It is in very good agreement with the PIV measurements for $Re_c \geqslant 150$. For $Re_c < 100$, it is lower than the PIV velocity, which is itself close to the bulk fluid velocity. This suggests that the migration of the tracers had not enough time to take place at low Reynolds numbers.

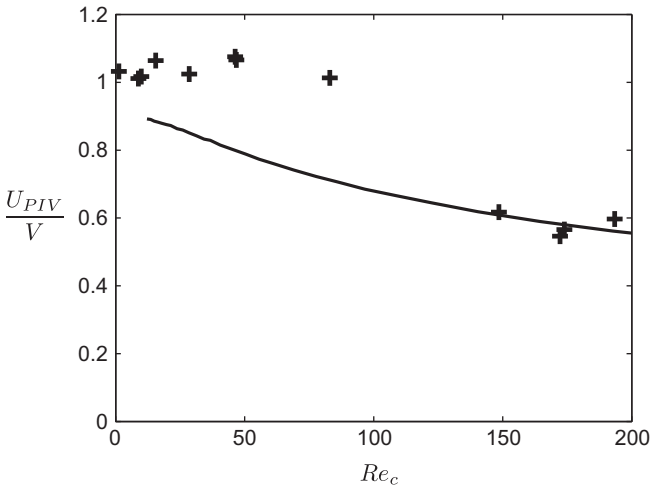

Fig. 6. Ratio U_{PIV}/V between the PIV velocity and the actual fluid velocity averaged over the gap: + experimental results, — theoretical prediction accounting for inertial migration of the tracers.

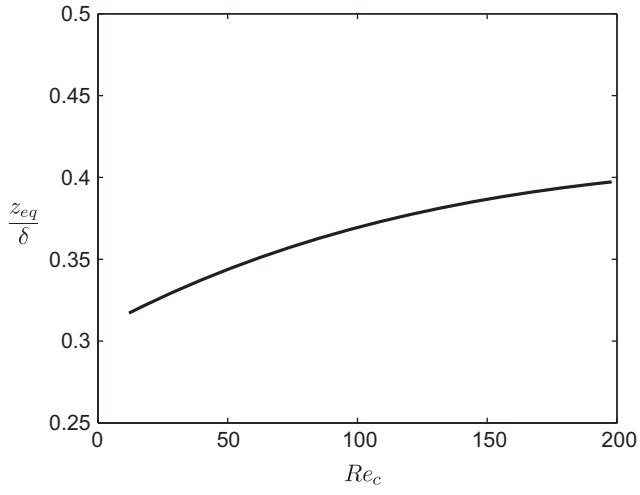

Fig. 7. Theoretical equilibrium position of a particle against the channel Reynolds number. This graph has been fitted from the data of Fig. 9 of Asmolov [1]: $z_{eq}/\delta = 3.0116 \times 10^{-9} Re_c^3 - 2.601 \times 10^{-6} Re_c^2 + 8.5141 \times 10^{-4} Re_c + 0.3073$.

We thus have to consider the time needed by the tracers to attain their equilibrium position. Asmolov [1] obtained the transverse lift force exerted on a particle as a function of its position z

$$F_{lift} = \frac{9}{4}\mu a\langle U\rangle Re_c^{-1/2} Re_p^{3/2} f_{Re_c}(z/\delta). \quad (2)$$

The transverse migration velocity, W, of the particle can be estimated from the equilibrium between the lift and the Stokes drag force. It writes

$$\frac{W}{\langle U\rangle} = \frac{3}{8\pi} Re_c^{-1/2} Re_p^{3/2} f_{Re_c}(z/\delta). \quad (3)$$

The function $f_{Re_c}(z/\delta)$, which cannot be expressed analytically, is drawn on Fig. 8 of the article of Asmolov [1] for various values of the channel Reynolds number ranging from 15 to 3000. In order to facilitate discussion, we have redrawn $f_{Re_c}(z/\delta)$ from Asmolov in the present system of coordinates in Fig. 8 for two Reynolds numbers. As observed on Fig. 7, the value of z_{eq} depends on Re_c. However, as shown in Fig. 8, f_{Rec} adopts an almost similar evolution on both sides of z_{eq} whatever the channel Reynolds number. The migration velocity is zero on the axis, which is an unstable equilibrium position for the tracers. Increasing z, f_{Rec} becomes positive (migration towards the wall), increasing first before to decrease and vanish at z_{eq}. The larger the Reynolds number, the flatter is the profile of the migration velocity in the central region and the smaller is its magnitude, which can be characterized by its maximum value: $1.5 \leqslant f_{max1}(Re_c) \leqslant 5.2$ for $10 < Re_c < 200$. Increasing z beyond z_{eq}, f_{Rec} becomes negative (migration towards the center) and decreases quickly to reach a maximum $f_{max2} \approx 28$ independent of Re_c at the wall. On both sides of z_{eq}, the tracers migrate toward the equilibrium position but the migration velocity is lower in the central region of the channel than in the wall region ($f_{max1}(Re_c) < f_{max2}$). Moreover, z_{eq} is moved towards the wall as Re_c increases, which makes the central region larger and larger while the wall region shrinks. A rough estimation of the time T_m taken by all the tracers to reach the stable equilibrium position can thus be estimated by taking $f_{Rec} = f_{max1} \approx 1$ as the magnitude of the migration velocity and z_{eq} as the distance of migration:

$$T_m = \frac{z_{eq}}{W} = \frac{8\pi}{3}\frac{z_{eq}}{\langle U\rangle} Re_c^{1/2} Re_p^{-3/2}. \quad (4)$$

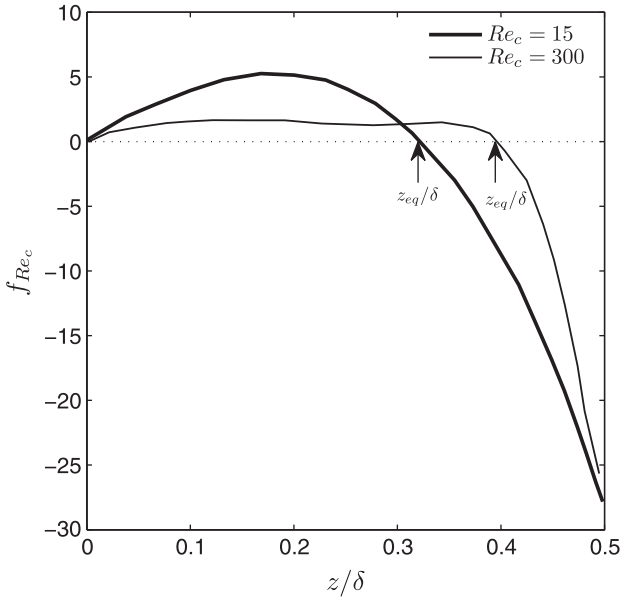

Fig. 8. Transverse profile of normalized lift force calculated by Asmolov. This graph has been constructed from the data of Fig. 8 of Asmolov [1]. (The origin $z/\delta = 0$ is at the channel center.)

The migration time T_m has now to be compared to the time T elapsed between the instant the flow is started by opening the discharging valve and the beginning of the calibration tests. We recall that T ranged between 2 s and 16 s, depending on the discharging velocity. Fig. 9 shows the evolution of the ratio T_m/T against Re_c for particles of three different diameters belonging to the range of the present tracer size distribution: $2a = 10$, 15 and 30 μm. For a given tracer size, the ratio T_m/T is observed to decrease strongly with the Reynolds number. For $Re_c \leqslant 80$ and whatever the tracer size, T_m/T is larger than 40, which might explain that the migration of the tracer does not affect the PIV measurements (Fig. 6). However, the estimated values of T_m/T for $Re_c \geqslant 150$ are still too large to argue that the migration has yet taken place at the instant the measurements are done. Indeed, it is only for the largest considered particles ($2a = 30$ μm) and for a Reynolds number close to 200 that T_m/T becomes smaller than 10. The theoretical prediction of the migration time is therefore overestimated. The exact effect of Re_c on the prediction of T_m/T from [1] is complex. Taking the upper limit of f_{max1} ($f_{max1} \approx 5$ at $Re_c = 15$) divides by 5 the value of T_m/T consistent with the migration observed at high Re_c. Several other reasons could also explain that migration modifies the velocity estimation at large Reynolds numbers while T_m/T is still of importance. First of all, it is important to note that the migration time decreases very strongly with the particle size since it scales as $(a/\delta)^{-3}$. Also, because the light fluoresced by a tracer particle is proportional to its volume, the contribution of a given tracer to the light intensity recorded on a PIV image is proportional to a^3. The larger particles, which are those that migrate the most rapidly, are therefore expected to influence the most the PIV measurements. Moreover, numerical simulations of inertial migration in a dilute particle suspension by Chun and Ladd [18] have shown that clusters of particles may appear for $Re_c > 200$. Since it has been observed that the present tracers can agglomerate when they are in contact, it is thus possible that the present particles agglomerate while they flow through cell to form larger tracers that migrate more rapidly. This effect is however expected not to be dominant because it was observed at higher tracer concentration as compared to our experimental conditions.

The present experiments conducted in a steady flow within a Hele-Shaw cell lead to the following conclusions. Inertial migration affects or not the PIV measurements depending on the time T elapsed after the Poiseuille flow has achieved its development across the gap. The migration time T_m decreases strongly when either the channel Reynolds number or the particle size increases.

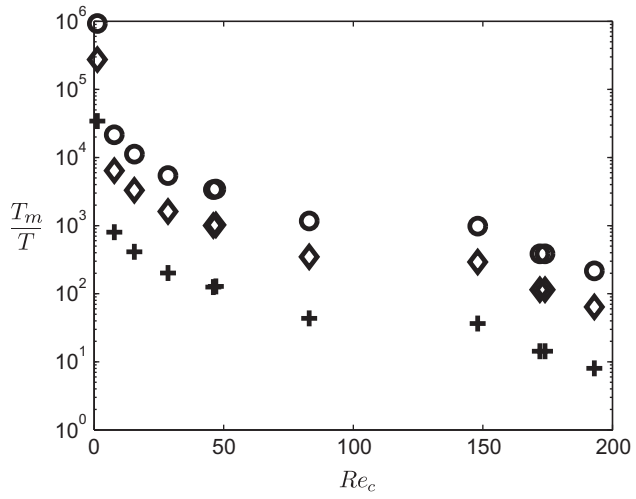

Fig. 9. Ratio T_m/T of the theoretical migration time over the experiment duration against the channel Reynolds number. ∘ $a = 5$ μm, △ $a = 7.5$ μm, + $a = 15$ μm.

In the present case, the PIV velocity is very close to the bulk fluid velocity V through the gap for $Re_c \leqslant 80$. The tracers remain thus probably almost uniformly distributed across the gap, they move at different velocity and the PIV algorithm provides the average flow velocity. Note that the PIV velocity is actually slightly larger than V for this range of Re_c, which may be due to the fact that slow particles close to the wall are expected to join quickly the equilibrium position since their migration velocity is large and independent of Re_c. On the other hand, for $Re_c \geqslant 150$, the PIV velocity corresponds exactly to the fluid velocity at the equilibrium position predicted by the Asmolov theory. In this case, the migration of the tracers is achieved and all the tracers have the same velocity, which is that of the flow at $z = z_{eq}$.

4. PIV measurements in rapidly varying flow

We will now consider PIV measurements of a flow which lasts for a finite time T. Different situations may occur depending on the relative magnitudes of T, of the viscous time scale $T_p = (\delta/2)^2/\nu$ and of the migration time T_m. The previous results suggest to distinguish the following cases:

(1) If $T < T_p$, the parabolic velocity profile does not have time to develop across the gap, the flow remains uniform in the z direction (except very close to the walls where thin boundary layers are present) and migration does not occur.
(2) If $T < T_m$, the migration of the tracers does not have time to occur, the parabolic profile being developed or not.
(3) If T is both larger than T_p and T_m the tracers have time to reach the equilibrium position z_{eq}.

Case (3) is equivalent to the steady case investigated in the previous section for $Re_c \geqslant 150$. Case (2) is similar to the situation of the previous section for $Re_c \leqslant 80$ where the flow was actually developed and steady but where the tracer migration was not completed. The purpose of this section is to deal with case (1) by investigating a flow that rapidly varies with time.

The reference situation chosen to test the response of the PIV system is the flow generated by a bubble rising at a velocity V_b in the Hele-Shaw cell. The bubble dynamics have already been investigated in details in [19] by means of high speed imaging for bubbles of equivalent diameter d ranging from 1 to 32.5 mm, which correspond to bubble Reynolds numbers, $Re_b = V_b d/\nu$, ranging from 62 to 7500 and channel Reynolds numbers, $Re_c = V_b\delta/\nu$, from 62 to 230. Here we consider a bubble with a diameter $d = 17$ mm rising at $V_b = 0.165$ m/s. The flow in the plane of the cell, characterized by $Re_b = 2800$, is dominated by inertia with a strong production of vorticity at the bubble surface leading to the development of an intense wake behind the bubble. The flow within the gap is characterized by a Reynolds number $Re_c = 165$ for which inertial migration was observed to affect the PIV measurements in the case of a steady flow. The time for developing a parabolic flow across the gap, $T_p = (\delta/2)^2/\nu \approx 0.25$ s, is larger than the duration of the flow, $T = d/V_b = 0.1$ s, suggesting that the velocity profile remains flat over the major part of the gap.

The flow field around the bubble has been measured by PIV as the bubble was crossing the measurement window. The right half of Fig. 10 shows an example of PIV velocity field. We observe that the bubble is pushing the fluid in front of its nose and entraining it at its rear. We will analyze separately the flows in the upstream region and in the wake because they are controlled by different physical mechanisms. Let us start by the flow upstream of the bubble. If the velocity profile across the gap is really flat, the flow in the cell plane (x,y) must be described well by the two-dimensional Navier–Stokes equations. Moreover, upstream of a bubble rising at large

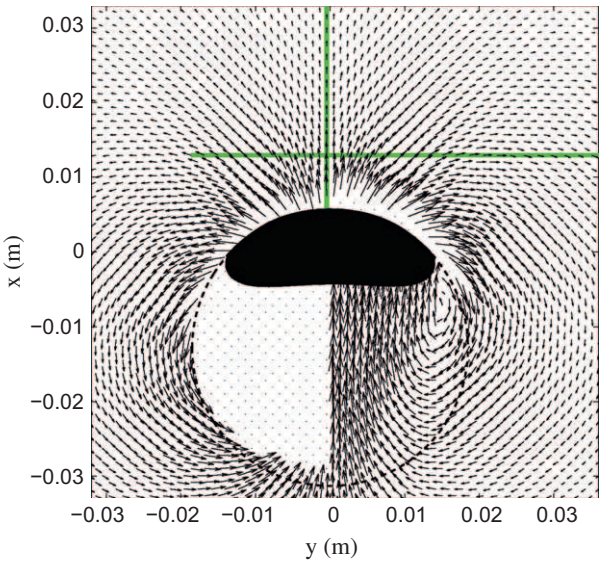

Fig. 10. Velocity field around a bubble of diameter $d = 0.017$ m rising at a velocity $V_b = 0.17$ m/s in the cell. Left half ($y < 0$), two-dimensional potential velocity generated by a moving circle. Right half ($y > 0$): PIV velocity.

Reynolds number, the flow is potential except in a thin boundary layer that develop at the interface. Also, it appears that the top half of the bubble interface has an almost constant curvature and is hence well described by a circle (dash line in Fig. 10). It is therefore relevant to compare the PIV measurements (right half of Fig. 10) with the two-dimensional potential flow generated by a circle moving at the same velocity as the bubble (left half of Fig. 10). Visual comparison of the map of velocity vectors shows a good agreement between PIV and potential theory. A more accurate comparison is proposed in Fig. 11, where the velocity profiles, taken along the two lines drawn in Fig. 10, are plotted. The quantitative agreement is excellent and allows us to conclude that the velocity profile across the gap is flat. There is therefore no ambiguity concerning the PIV velocity.

Let us now consider the flow behind the bubble. Fig. 12 shows the streamlines of the velocity field in the frame moving with the bubble computed from the PIV data. In contrast with the upstream region, we have no theoretical prediction of the two-dimensional velocity field in the wake. However, we observe at the bubble rear a closed streamline which separates a recirculating region in which the liquid is rising with the bubble from the outer flow. As a consequence, the liquid velocity averaged on any horizontal line segments within the attached wake must be equal to the bubble rise velocity V_b. This average velocity U_w has been calculated from the PIV velocity field $U_{PIV}(x,y)$ by using the following equation:

$$U_w(x) = \frac{1}{2Y(x)} \int_{Y(x)}^{-Y(x)} U_{PIV}(x,y)dy, \tag{5}$$

where $-Y(x)$ and $Y(x)$ are the horizontal coordinates of the closed streamline for the considered vertical coordinate x (the origin corresponding to the bubble centre). For $x = -12$, -16 and 20 mm, we obtain respectively $U_w/V_b = 1.02$, 1.03 and 1.01. Similarly to what is observed from the local description of the flow upstream of the bubble, the duration of the flow $T = x/V_b \leqslant 0.15$ s is too short to allow the development of a parabolic profile across the gap and the PIV provides the actual fluid velocity.

5. Conclusion

Methods for liquid velocity measurements in narrow channels using particle as flow tracers have to deal with two major difficul-

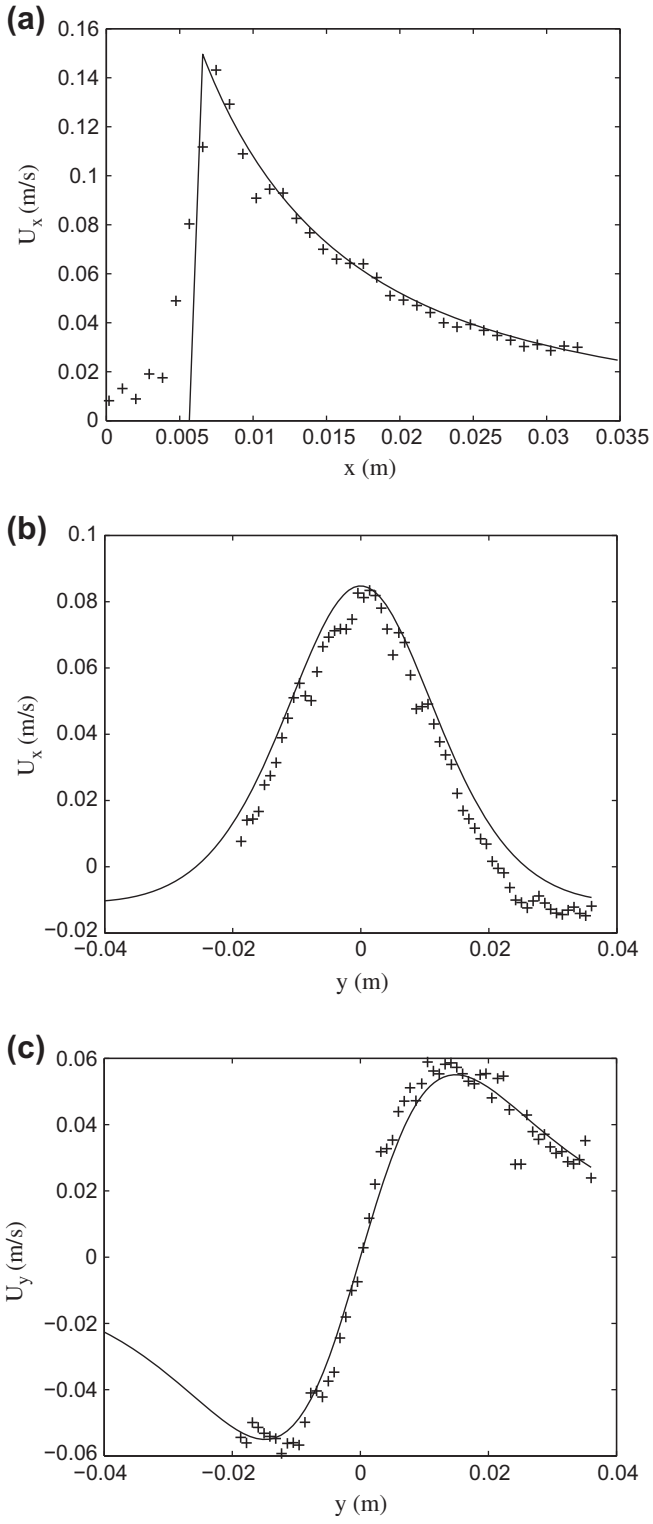

Fig. 11. Velocity profiles upstream of the bubble along the lines marked on Fig. 10: (a) vertical velocity along $y = 0$, (b) vertical velocity along $x = 0.012$ m and (c) horizontal velocity along $x = 0.012$ m. Symbols denote PIV measurements while curves represent potential theory.

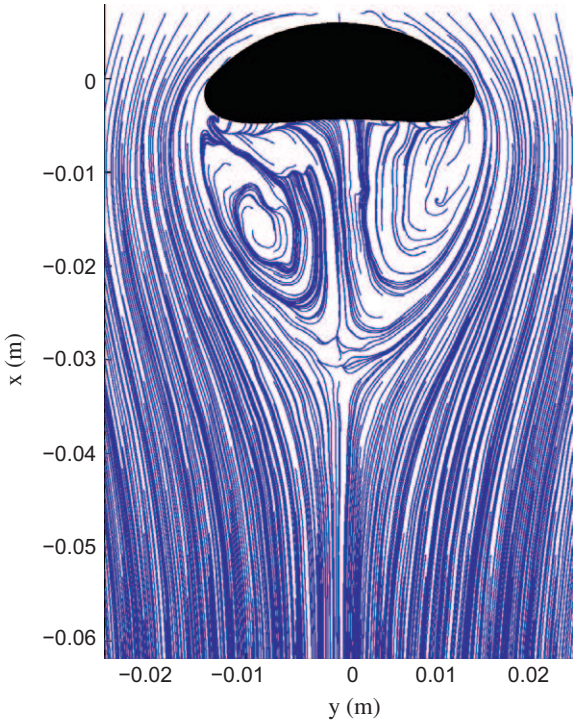

Fig. 12. Streamlines of the liquid flow around the rising bubble (represented in the frame that moves with the bubble).

ties: strong velocity variations occur on short distances in the direction perpendicular to the walls and inertial migration may cause non-uniform spatial distribution of the tracers. It is particularly true for PIV when using volume illumination and an optical depth of field larger than the channel thickness because the tracer positions within the gap are not known. The purpose of the present work was to test this particular PIV method by considering reference flows for which the velocity field is known by an independent way. The results obtained here allow us to draw guidelines for the use of this method in confined flows when using neutrally buoyant tracers that are negligibly small compared to the gap δ. Three contrasted situations have to be distinguished. On the one hand, when the flow duration is short compared to the time, $T_p = (\delta/2)^2/\nu$, required for the vorticity generated at the wall to diffuse into the core of the flow, the velocity profile across the gap remains flat, all the tracers travel at the same velocity, which is therefore the one measured by the PIV method. On the other hand, when the flow duration is long enough, a parabolic profile develops across the gap and the tracers start moving towards a stable equilibrium position located at a certain distance to the wall where they will eventually accumulate. The PIV measurements will then be different according to whether the tracers have time to migrate before the instant the measurement is done. If the migration time is large, the tracers do not have time to move and remain thus uniformly distributed, which implies that each tracer moves at a velocity that depends on its distance to the wall. In this case, the present experimental results show that the PIV provides the liquid velocity averaged over the gap. It is worth noting that this empirical result is not trivial since the image intercorrelation used by the PIV algorithm is not an average operator. If the migration time is short, all the tracers have ceased their migration at the instant of measurement and therefore all move at the same velocity, which is that of the flow at the equilibrium position. The fluid velocity averaged over the gap can then be determined with a good accuracy from the PIV measurement by using the theoretical prediction of the equilibrium position derived by Asmolov [1]. Concerning the migration velocity, the theory predicts that it strongly depends on both the channel Reynolds number and the tracer size. That might explain why an estimation of the migration time based of the theoretical migration velocity does not allow us to discriminate between the two last

cases. Further work is needed to propose a reliable method to predict precisely the migration time for practical applications. However we showed that there are many situations in which tracers migration did not occur. In particular the present method is well suited to investigate the flow generated by confined bubbles.

Acknowledgements

We would like to thank S. Cazin and E. Cid for their help in instrumentation and the FERMaT federation of laboratories for financial support.

References

[1] E.S. Asmolov, The inertial lift on a spherical particle in a plane Poiseuille flow at large channel Reynolds number, J. Fluid Mech. 381 (1999) 63–87.
[2] D. Sinton, Microscale flow visualization, Microfluid. Nanofluid. 1 (2004) 2–21.
[3] S.T. Wereley, Meinhart recent advances in micro-particle image velocimetry, Annu. Rev. Fluid Mech. 42 (2010) 557–576.
[4] J. Westerweel, Fundamentals of digital particle image velocimetry, Meas. Sci. Technol. 8 (1997) 1379–1392.
[5] C. Tropea, A.L. Yarin, J.F. Foss (Eds.), Springer Handbook of Experimental Fluid Mechanics, Springer, 2007.
[6] C.D. Meinhart, S.T. Wereley, J.G. Santiago, PIV measurements of a microchannel flow, Exp. Fluids 27 (1999) 414–419.
[7] C.D. Meinhart, S.T. Wereley, M.H.B. Gray, Volume illumination for two-dimensional particle image velocimetry, Meas. Sci. Technol. 11 (2000) 809–814.
[8] E.B. Cummings, An image processing and optimal nonlinear filtering tech for PIV of microflows, Exp. Fluids 29 (Suppl.) (2001) 42–50.
[9] M.G. Olsen, R.J. Adrian, Out-of-focus effects on particle image visibility and correlation in microscopic particle image velocimetry, Exp. Fluids 7 (Suppl.) (2000) 166–174.
[10] J. Westerweel, On velocity gradients in PIV interrogation, Exp. Fluids 44 (2008) 831–842.
[11] G. Segre, A. Silberberg, Behaviour of macroscopic rigid spheres in Poiseuille flow. Part 2, Exp. Results Interpretation 14 (1962) 136–157.
[12] B. Lecordier, D. Demare, L.M.J. Vervisch, J. Rveillon, M. Trinit, Estimation of the accuracy of PIV treatments for turbulent flow studies by direct numerical simulation of multi-phase flow, Meas. Sci. Technol. 9 (2001) 1382–1391.
[13] E. Cid, F. Gardelle, Manuel d'utilisation du logiciel PIVIS, Inst Méc Fluides Toulouse (2005).
[14] P.G. Saffman, On the motion of small spheroidal particles in a viscous liquid, J. Fluid Mech. 1 (1956) 540–553.
[15] J.A. Schonberg, E.J. Hinch, Inertial migration of a sphere in Poiseuille flow, J. Fluid Mech. 203 (1989) 517–524.
[16] J-P. Matas, J.F. Morris, E. Guazzelli, Inertial migration of rigid spherical particles in Poiseuille flow, J. Fluid Mech. 515 (2004) 171–195.
[17] Y.W. Kim, J.Y. Yoo, The lateral migration of neutrally-buoyant spheres transported through square microchannels, J. Micromech. Microeng. 18 (2008) 1–13.
[18] B. Chun, A.J.C. Ladd, Inertial migration of neutrally buoyant particles in a square duct: an investigation of multiple equilibrium positions, Phys. Fluids 18 (2006) 1–4.
[19] M. Roudet, V. Roig, A.M. Billet, F. Risso, Paths and shapes of two-dimensional rising bubbles at high-Reynolds number, in: Multiphase Flows ICMF07, 9–13 July, Leipzig, Germany, 2007.